

THE UNUSUAL DISTRIBUTIONS OF IONIZED MATERIAL AND MOLECULAR HYDROGEN IN NGC 6881: SIGNPOSTS OF MULTIPLE EVENTS OF BIPOLAR EJECTION IN A PLANETARY NEBULA

RAMOS-LARIOS, G.¹

Instituto de Astronomía y Meteorología, Av. Vallarta No. 2602, Col. Arcos Vallarta, C.P. 44130 Guadalajara, Jalisco, México; gerardo@astro.iam.udg.mx

GUERRERO, M.A. AND MIRANDA, L.F.

Instituto de Astrofísica de Andalucía, IAA-CSIC, C/ Camino Bajo de Huétor 50, 18008 Granada, Spain; mar@iaa.es, lfm@iaa.es

To be published in The Astronomical Journal

ABSTRACT

The planetary nebula NGC 6881 displays in the optical a quadrupolar morphology consisting of two pairs of highly collimated bipolar lobes aligned along different directions. An additional bipolar ejection is revealed by the hydrogen molecular emission, but its wide hourglass morphology is very different from that of the ionized material. To investigate in detail the spatial distribution of molecular hydrogen and ionized material within NGC 6881, and to determine the prevalent excitation mechanism of the H₂ emission, we have obtained new near-IR Br γ and H₂ and optical H α and [N II] images, as well as intermediate resolution *JHK* spectra. These observations confirm the association of the H₂ bipolar lobes to NGC 6881 and find that the prevalent excitation mechanism is collisional. The detailed morphology and very different collimation degree of the H₂ and ionized bipolar lobes of NGC 6881 not only imply that multiple bipolar ejections have occurred in this nebula, but also that the dominant shaping agent is different for each bipolar ejection: a bipolar stellar wind most likely produced the H₂ lobes, while highly collimated outflows are carving out the ionized lobes into the thick circumstellar envelope. The asymmetry between the southeast and northwest H₂ bipolar lobes suggests the interaction of the nebula with an inhomogeneous interstellar medium. We find evidence that places NGC 6881 in the H II region Sh 2-109 along the Orion local spiral arm.

Subject headings: infrared: ISM: continuum — ISM: molecules — planetary nebula: individual (NGC 6881)

1. INTRODUCTION

Asymmetry is common among planetary nebulae (PNe) and it comes in a large variety of shapes and morphological features. On a large scale, the departure from symmetry goes from the mild asymmetry of elliptical PNe to the strong asymmetry displayed by bipolar PNe. Asymmetry in PNe is also revealed by an assortment of small-scale morphological features including the symmetric fast low-ionization emission regions (FLIERS) of elliptical PNe, as well as point-symmetric collimated outflows and their associated blowouts and bow-shock structures. The asymmetry in PNe has been linked on many occasions to binarity (e.g., Soker 2006), but there is no conclusive evidence supporting such connection (Sörensen & Pollacco 2004; Bond 2000; Soker 1997, and references therein). On the contrary, the onset of bipolarity in PNe seems to require the evolution of a massive progenitor (e.g., Corradi & Schwarz 1995).

PNe that show asymmetric structures along different directions are of great importance, as the change in the direction of the ejection can be associated with the precession of the progenitor star in a binary system. This class of PNe is not homogeneous at all, and includes PNe with multiple collimated outflows along different directions (Corradi et al. 1997) or with precessing jet-like features (Miranda, Guerrero & Torrelles 1999), starfish-shaped and multipolar PNe that show point-symmetric bow-shock features (Sahai & Trauger 1998; Sahai 2000),

and quadrupolar and polypolar PNe with different sets of bipolar lobes aligned along different symmetry axes (Manchado, Stanghellini & Guerrero 1996; López et al. 1998). Polypolar and quadrupolar PNe are especially interesting as multiple hourglass structures imply recurrent bipolar ejections which are particularly difficult to interpret in the framework of the interacting stellar wind model (Kwok, Purton & Fitzgerald 1978; Balick 1987).

One of the most intriguing PNe with multiple bipolar lobes is NGC 6881. Originally classified as a quadrupolar PN, based on optical narrowband images and long-slit echelle spectra (Guerrero & Manchado 1998), NGC 6881 presents two pairs of highly collimated bipolar lobes with very similar, although not coincident, symmetry axes. The southwest lobe displays a loop-like feature that is highly reminiscent of a precessing collimated outflow, but its measured expansion velocity is low. Kwok & Su (2005) showed that the dense equatorial ring has recently changed its orientation, being aligned with the youngest pair of bipolar lobes.

Therefore, there are many signs suggesting that precession and sequential events of bipolar ejections have occurred in NGC 6881. The spatial distribution of the molecular hydrogen in this nebula, as revealed by near-IR narrowband H₂ (1–0) S(1) images (Guerrero et al. 2000), adds a new twist. Molecular hydrogen emission is detected in wide hourglass bipolar lobes that extend much farther than the ionized bipolar lobes. The H₂ bipolar lobes may represent a bipolar ejection unrelated to the formation of the two pairs of ionized bipolar lobes.

¹ Visiting Astronomer, Instituto de Astrofísica de Andalucía.

TABLE 1
NARROW-BAND IMAGING OF NGC 6881

Telescope	Filter	λ_c (Å)	$\Delta\lambda$ (Å)	Exp. Time (s)
WHT	H ₂ (1–0)	21218	320	900
WHT	Br γ	21658	320	1000
WHT	Kc	22700	340	1000
NOT	[N II]	6589	9	1800
NOT	H α	6568	8	900

To study carefully the spatial distributions of ionized material and molecular hydrogen in NGC 6881 and to investigate the excitation mechanism of the H₂ molecule throughout the nebula, we have obtained new H₂, Br γ , [N II], and H α images, and *JHK* intermediate-resolution long-slit spectroscopic observations. A description of the observations is presented in §2 and the results are given in §3. The results are discussed in §4, and the conclusions and a short summary are presented in §5.

2. OBSERVATIONS

2.1. Imaging

Narrowband near-IR images of NGC 6881 were obtained during 2006 September 9 using LIRIS (Long-Slit Intermediate Resolution Infrared Spectrograph) at the Cassegrain focus of the 4.2 m William Herschel Telescope (WHT) on Roque de Los Muchachos Observatory (ORM, La Palma, Spain). The detector was a 1k×1k HAWAII array sensitive in the spectral range from 0.8 to 2.5 μ m. The plate scale is 0''.25 pixel⁻¹ and the field of view (FOV) is 4'.27×4'.27. The narrowband filters isolated the H₂ (1–0) S(1) 2.1218 μ m and Br γ 2.1658 μ m emission lines. An additional narrowband filter (Kc) centered at 2.270 μ m was used in order to subtract the continuum contribution from the line emission detected through the H₂ and Br γ filters. The central wavelength and bandwidth of these filters are listed in Table 1.

We obtained series of 100 s exposures on each filter for the total integration times given in Tab. 1. The telescope pointing was shifted by a few pixels between each exposure, rastering the nebula to different locations on the detector. Each series of observations on the object was followed by a similar series of observations on adjacent blank sky positions. Individual exposures were flat-fielded and dark-corrected, and the sky frames were combined to obtain a master sky image. The images on the nebula were subsequently sky-subtracted, shifted, and averaged. The continuum contribution to the H₂ and Br γ emission was removed using the continuum Kc image. Since the H₂, Br γ , and Kc filters have very similar bandwidth, we do not find it necessary to scale the images, although differences in the point-spread function (PSF) of stars in the field of view required us to degrade the PSF of the H₂ image to match these of the Br γ and Kc images. The continuum subtracted H₂ and Br γ images and the Kc image are presented in Figure 1. The spatial resolution, as determined from the FWHM of stars in the FOV, is \sim 0''.8.

Narrowband images in the [N II] and H α emission lines were obtained on 2006 June 30 using ALFOSC (Andalucia Faint Object Spectrograph and Camera) at the 2.56 m Nordic Optical Telescope (NOT) in the ORM. The camera is a 2048×2048 CCD with a plate scale of

TABLE 2
NIR SPECTROSCOPIC OBSERVATIONS OF NGC 6881

Grism	λ (μ m)	Dispersion (Å pix ⁻¹)	Slit Width (")	R	PA (°)	Exp time (s)
<i>JH</i>	1.15–1.75	6.6	0.75	\sim 575	113	1800
<i>K_B</i>	1.92–2.34	4.3	0.75	\sim 1700	113	3000
<i>K_B</i>	1.92–2.34	4.3	0.75	\sim 1700	137	1200

0''.19 pixel⁻¹ and a FOV of 6'.5×6'.5. The [N II] and H α images of NGC 6881 are also presented in Fig. 1. The spatial resolution, as determined from the FWHM of stars in the FOV, was 0''.9.

2.2. Spectroscopy

Intermediate-resolution *JHK* long-slit spectroscopic observations were performed on 2004 July 2–4 using the NICS (Near Infrared Camera Spectrometer) at the 3.5 m Telescopio Nazionale Galileo (TNG) at the ORM. The NICS is a multimode instrument for IR observations (0.9–2.5 μ m) that uses a HAWAII 1024 × 1024 array as detector. We used the LF camera, providing a plate scale of 0''.25 pixel⁻¹, and the 0.75 slit, with a width of 0''.75 and a length of 4'. Observations were obtained using the *JH* and *K_B* grisms and the long-slit was placed along the central star at P.A.s 113° and 137° (Table 2). In order to provide the means for subtracting the sky emission, the nebula was placed at different positions along the slit.

The spectra were reduced using IRAF² routines of the noao.twodspec and noao.onedspec packages. The data were flat-fielded using dome flats, and the sky contribution was removed using sky spectra obtained at the same time as the nebular spectra. We used telluric sky lines for the wavelength calibration. The standard IR stars of spectral type A–A0 SAO 15832, SAO 48300, and SAO 72320 (Hunt et al. 1998) were used for the flux calibration. We obtained the sensitivity function by comparing the spectra of these stars with a blackbody model of temperature 9480 K, similar to the effective temperature of A0 stars. Finally, the telluric absorptions in the one-dimensional spectra of NGC 6881 were removed using the IRAF task “telluric”, applying it to stars with featureless spectra in the *JHK* range.

3. RESULTS

3.1. Morphology

The notable differences in the spatial distributions of ionized material and molecular hydrogen within NGC 6881 described by Guerrero et al. (2000) are specially highlighted in the H₂, H α , and [N II] composite picture shown in Figure 2. In NGC 6881, we can distinguish the following components.

3.1.1. The Equatorial Torus at the Central Region

The central regions of NGC 6881 contain both molecular and ionized material. This region can be described as a clumpy torus-like structure (Kwok & Su 2005) that is expanding at a moderate velocity

² IRAF is distributed by the National Optical Astronomy Observatory which is operated by the Association of Universities for Research in Astronomy, Inc. under cooperative agreement with the National Science Foundation

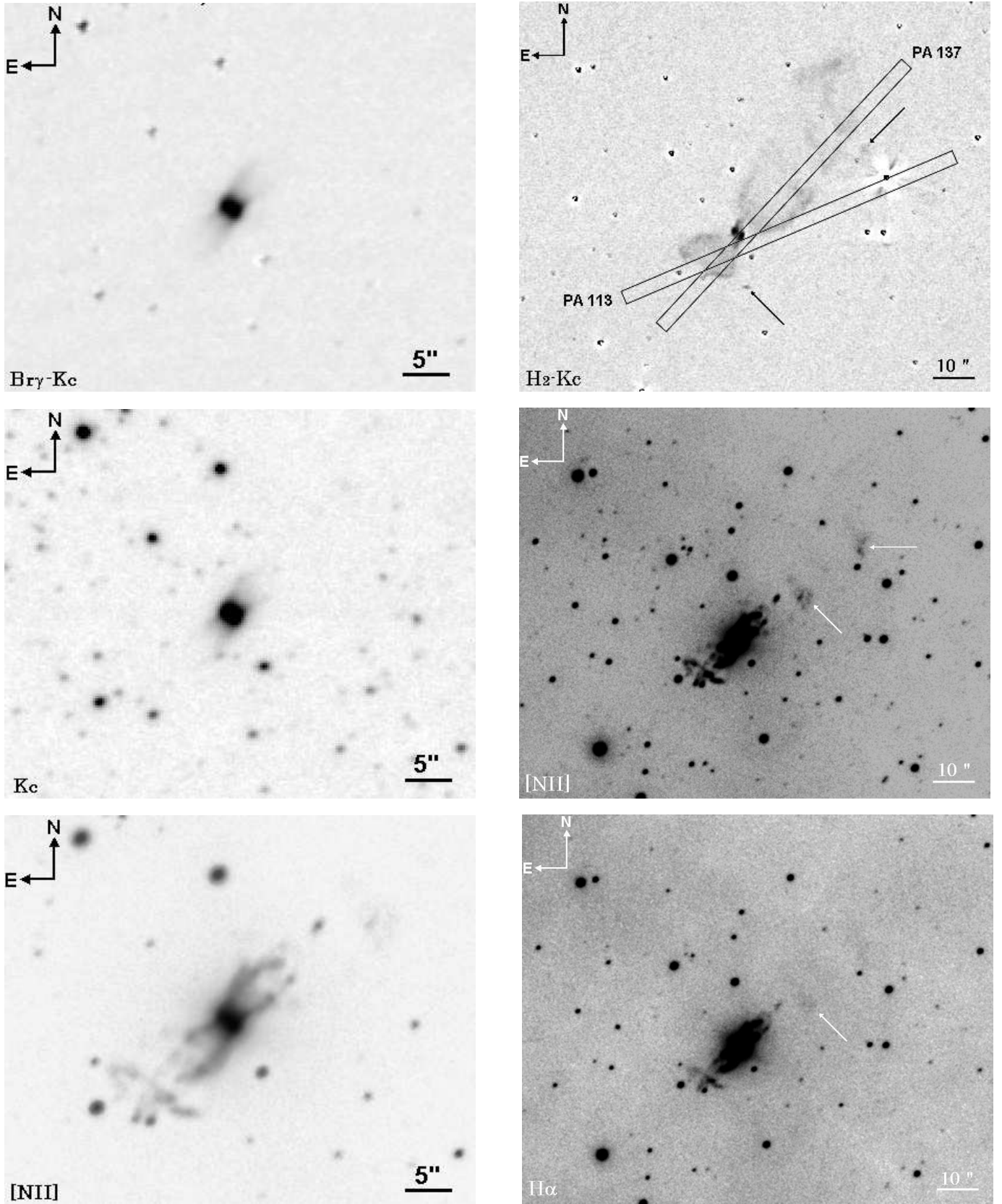


FIG. 1.— Images of NGC 6881 in the $\text{Br}\gamma$ (top, left), Kc (middle, left), and $[\text{N II}]$ (bottom, left) narrowband filters. The images in the H_2 (top, right), $[\text{N II}]$ (middle, right) and $\text{H}\alpha$ (bottom, right) filters show a larger field of view than the images in the left column. The artifacts noticeable around the field stars in the continuum subtracted $\text{Br}\gamma$ and H_2 images are residuals of the subtraction caused by a slight mismatch of the PSF between the line and continuum images. The arrows towards the northwest of the nebula in the right panels mark diffuse emission in the H_2 , $[\text{N II}]$, and $\text{H}\alpha$ images associated with the northwest H_2 lobe and its northwest extension. The arrow towards the south of the nebula in the H_2 image marks diffuse emission unrelated to NGC 6881, probably a background galaxy.

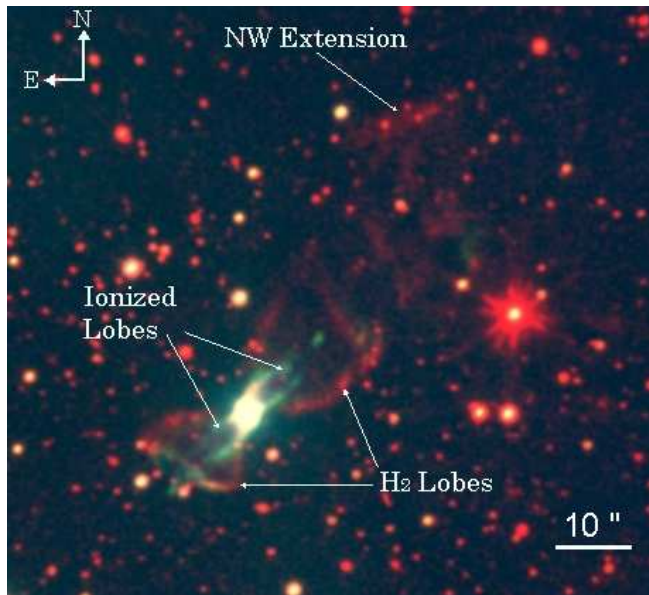


FIG. 2.— WHT LIRIS H_2 (red), and NOT ALFOSC $H\alpha$ (blue) and $[N II]$ (green) composite picture of NGC 6881 overlaid with the different morphological features identified in the nebula.

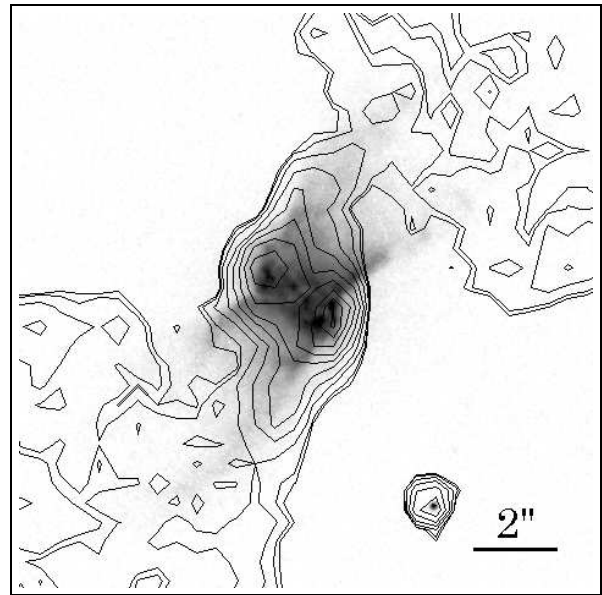


FIG. 3.— Expanded view of the central region of NGC 6881 in the *HST* WFPC2 $[N II]$ image. The image is overlaid with H_2 contours extracted from the WHT LIRIS continuum-subtracted H_2 image.

(Guerrero & Manchado 1998). The details of the molecular and ionized material distribution in the central regions of NGC 6881, however, could not be studied properly by Guerrero et al. (2000), because of the limited spatial resolution of their near-IR images and poor continuum subtraction at this region. Our new continuum-subtracted H_2 image reveals two bright knots of H_2 emission located at the central region of NGC 6881 along its minor axis, suggesting a ring of molecular material. The relative distribution of ionized and molecular material in the central region of NGC 6881, shown in Figure 3, reveals that the H_2 emission encompasses the $[N II]$ emission.

Molecular hydrogen in this region survives in a thin layer surrounding the ionized torus-like structure, most likely shielded by dense material from the ionizing flux of the central star.

3.1.2. The Highly Collimated Bipolar Lobes

The two pairs of highly collimated bipolar lobes are mainly detected in the $Br\gamma$, $[N II]$, and $H\alpha$ images, while the H_2 emission from these lobes is weak. The northern wall of the northwest lobe is brighter than its southern wall, and the opposite applies to the southeast lobe, thus showing the point-symmetric brightness distribution typical of other bipolar PNe (e.g., K 4-55, Guerrero et al. 1996).

3.1.3. The Hourglass H_2 Bipolar Lobes

Contrary to the highly collimated bipolar lobes, the open hourglass bipolar lobes of NGC 6881 are dominated by H_2 emission.

They show a narrow waist coincident with NGC 6881 central regions and clear limb-brightening, indicating that they are formed by a thin layer of material.

The southeast lobe, extending $\sim 12''$, is smaller than the northwest lobe, with a size up to $\sim 20''$. There are notable differences between the tips of the southeast and

northwest lobes. The tip of the southeast lobe is sharp and can be associated with the southeast loop-like structure detected in $H\alpha$ and very prominently in $[N II]$ (Figure 4). The westernmost emission of the $[N II]$ loop is coincident with the southwestern elbow of the H_2 lobe, and the $[N II]$ loop structure traces closely the edge of the H_2 lobe. The northwest lobe does not have a sharp edge nor does it displays a loop-like structure, but only a knot and a thin filament visible in the $[N II]$ image located at its Westernmost tip (Figs. 1 and 2).

3.1.4. The Northwest Bipolar Lobe Extension

The H_2 emission of the northwest hourglass lobe displays an extension that casts its emission outwards up to $\sim 50''$ from the center of NGC 6881 along its symmetry axis. This emission is mainly detected in H_2 , but there are also hints of $[N II]$ and $H\alpha$ emission (Fig. 2). The H_2 surface brightness of this feature is not homogeneous, but is distributed on a series of three bright bands interspersed between bands of diminished brightness. Interestingly, the bright bands can also be recognized in the $H\alpha$ image. The northwesternmost tip of these bands shows a remarkable wedge-shaped morphology.

3.1.5. Large-Scale Emission

The $H\alpha$ and $[N II]$ images of NGC 6881 show large-scale diffuse emission, with the nebula laying on a broad arc of patchy emission that crosses the FOV from the northeast to the south (Fig. 1). An examination of an $H\alpha$ image from the INT/WFC Photometric $H\alpha$ Survey (IPHAS) of the northern Galactic plane (Drew et al. 2005) of this region reveals a complex system of filaments. NGC 6881 ($l=74^\circ 55' 20''$, $b=+02^\circ 11' 37''$) is projected along the local spiral arm onto the intricate network of $H\alpha$ filaments near the proximity of γ Cyg (e.g., Parker, Gull, & Kirshner 1979). In particular, NGC 6881 is projected towards the east of a large cavity

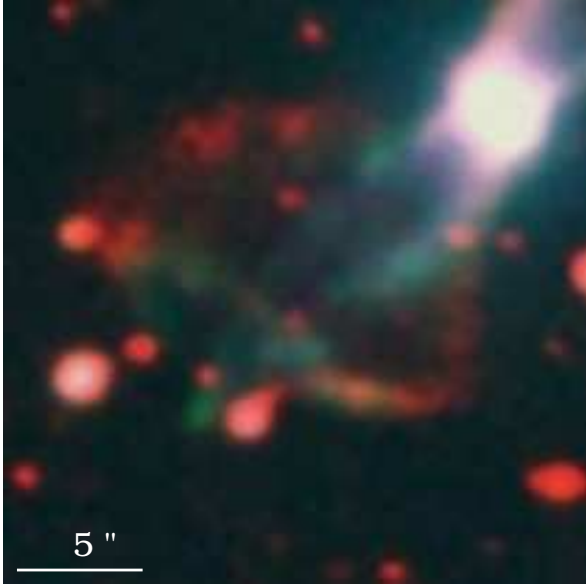


FIG. 4.— Expanded view of the southeast loop-like feature from the H_2 , $H\alpha$, and $[N II]$ composite picture of NGC 6881 (Fig. 2).

TABLE 3
LINE FLUXES AT P.A. 137° WITH K_B GRISM

λ [Å]	Line ID	Regions			
		Central Regions	Ionized lobes	H_2 lobes	NW H_2 lobe extension
		[$\times 10^{15}$ ergs cm^{-2} s^{-1} Å $^{-1}$]			
19446	Br 8 H I	63
19549	He I	16
19574	H_2 (1,0) S(3)	12	17	11	9.2
19703	H_2 (8,6) O(2)	2.1
20338	H_2 (1,0) S(2)	4.2	2.1	3.8	4.6
20377	?	4.7
20587	He I	47	1.3	0.4	2.4
20732	H_2 (2,1) S(3)	1.2	0.8	1.3	2.8
20763	?	0.9
21126	He I	5.1
21138	He I	2.2
21218	H_2 (1,0) S(1)	12	4.7	5.6	6.2
21542	H_2 (2,1) S(2)	0.4
21614	He I ?	2.9
21658	Br 7 H I (Brg)	110	5.5	1.3	...
21793	Br I	1.1
21887	He II	17	0.8
21985	?	2.1
22235	H_2 (1,0) S(0)	3.3	1.2	...	1.5
22477	H_2 (2,1) S(1)	1.6	1.0
22872	Br I ?	7.1

of size $20' \times 12'$ oriented along the north-south direction that forms part of the H II region Sh 2-109 ($l = 79^\circ 48$, $b = +00^\circ 15$).

3.2. Spectroscopic Analysis

The long-slit spectra of NGC 6881 detect continuum emission from the innermost regions and extended line emission all through the nebula. A preliminary inspection of the two-dimensional spectra reveals the variation at different locations of the nebula of important line ratios (e.g. H_2 1–0 S(1)/Br γ , He I/He II), in agreement with the different spatial distribution of emission shown

TABLE 4
LINE FLUXES JH AND K_B GRISMS AT PA 113°

λ [Å]	Line ID	Regions	
		Ionized Lobes [$\times 10^{15}$ ergs cm^{-2} s^{-1} Å $^{-1}$]	H_2 Lobes [$\times 10^{15}$ ergs cm^{-2} s^{-1} Å $^{-1}$]
10936	Pa 6 H I	160	...
11621	C I ? + Fe I ?	21	...
11666	H_2 (3,1) S(4), He I ?	4.5	...
11892	H_2 (2,0) S(0)	21	...
11970	He I	4.0	...
12566	[Fe II] ?, + Fe II ?	33	1.2
12784	He I	13	...
12817	Pa 5 (PaB) H I	190	11
13202	?	13	...
15335	Br 18 H I	2.3	...
15549	Br 16 H I	1.2	...
15693	Br 15 H I, H I 4-15	1.2	...
15875	Br 14 H I	1.1	...
15995	[Fe II]	1.0	...
16102	Br 13 H I, H I 4-13	2.5	...
16401	Br 12 H I, H I 4-12	2.6	...
16432	[Fe II]	15	...
16763	?	1.7	...
16801	Br 11 H I, H I 4-11, Fe I ?	3.9	...
16997	He I	2.5	...
17356	Br 10 H I	5.5	...
17478	H_2 (1,0) S(7)	1.9	10
19570	H_2 (1,0) S (3) + [Fe II] ?	17	61
19703	H_2 (8,6) O (2)	1.1	...
20338	H_2 (1,0) S(2)	3.0	7.7
20580	He I	4.6	...
20656	H_2 (3,2) S(5)	0.5	...
20732	H_2 (2,1) S(3)	0.8	...
21133	He I	0.7	1.6
21218	H_2 (1,0) S (1)	6.8	11
21658	Br 7 (Brg) H I	7.4	0.9
21892	He II	0.9	...
21986	?	0.7	1.0
22014	H_2 (3,2) S(3)	1.0	...
22235	H_2 (1,0) S(0)	2.3	4.7
22477	H_2 (2,1) S(1)	1.2	1.7
22870	H_2 (3,2) S(2)	1.0	1.8

by the Br γ and H_2 images. Guided by these images, we have extracted spectra from four individual regions: the central region, the ionized lobes, the H_2 -dominated hourglass lobes, and the northwest H_2 lobe extension. The K spectra of these regions are shown in Figure 5, and the JHK spectra of the ionized lobes in Figure 6. Within our limited spectral resolution, the radial velocity derived for the different regions is similar.

The measured line intensities are listed in Table 3 and 4. The spectra and line ratios confirm that the central region is Br γ -dominated, the ionized lobes show H_2 /Br γ ~ 1 , and the outermost regions are H_2 -dominated. He II emission is confined to the central region, while the outermost regions show a wealth of H_2 lines. We note that the spectrum from the ionized lobes is most likely contaminated by emission from the H_2 -dominated hourglass lobes.

3.3. H_2 Excitation

The molecule of H_2 can be excited by shocks or by UV fluorescence. The 1–0 S(1)/2–1 S(1) line ratio is traditionally used to diagnose the H_2 excitation mechanism, with a line ratio ~ 2 implying UV fluorescence

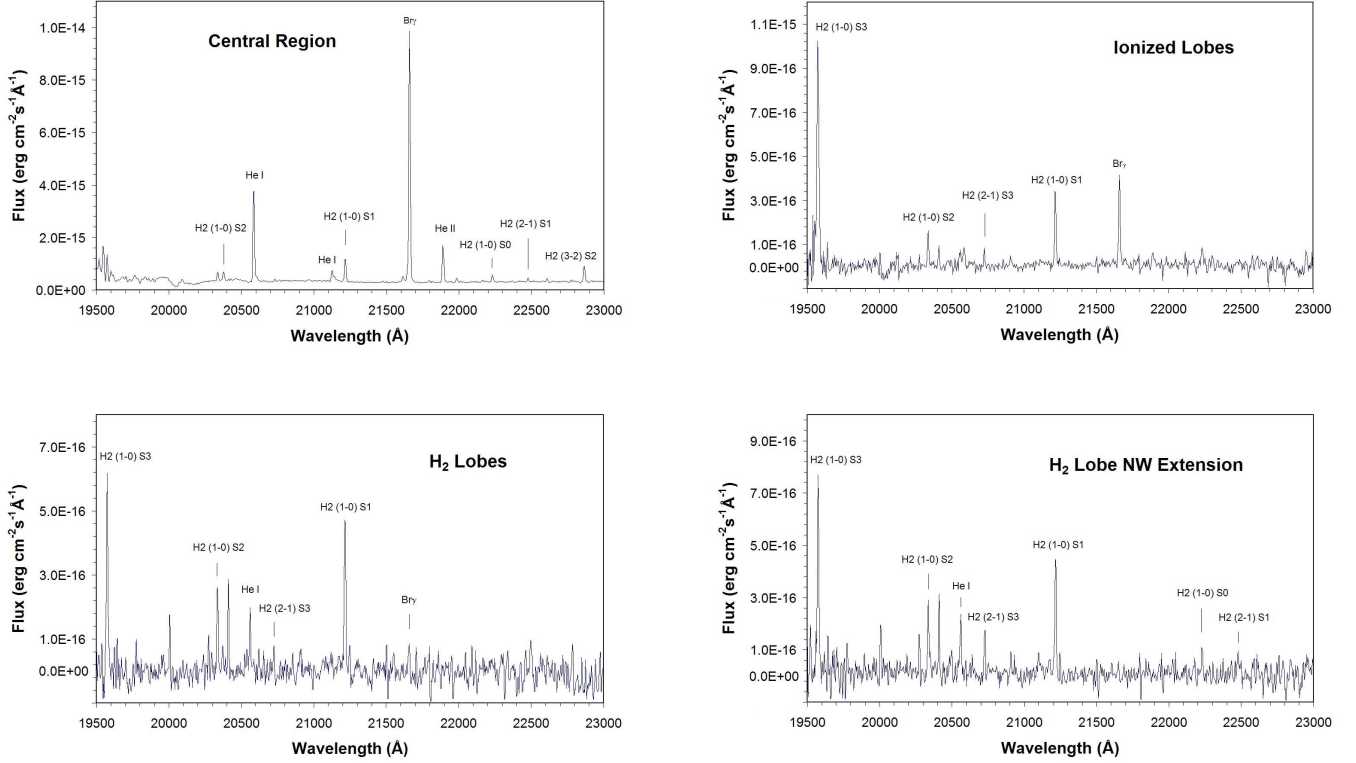


FIG. 5.— K_B spectra along P.A. = 137° of the central region, ionized lobes, H_2 -dominated bipolar lobes, and northwest extension of the northwest H_2 bipolar lobe of NGC 6881. Line identifications are overlaid on the spectra.

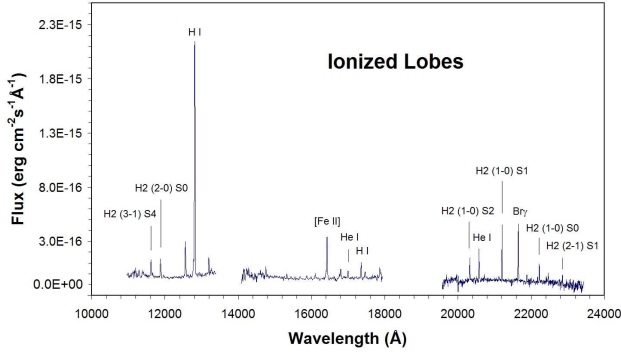


FIG. 6.— J , H , and K_B spectra along P.A. = 113° of the ionized lobes of NGC 6881. Line identifications are overlaid on the spectra.

(Black & van Dishoeck 1987), and a line ratio ~ 10 implying shock excitation (Burton et al. 1989). The $1-0 \text{ S}(1)/2-1 \text{ S}(1)$ line ratio in the different regions of NGC 6881 ranges from 5.5 up to 7.5, thus indicating that shock excitation can be the most likely dominant excitation mechanism.

In a case of pure collisional excitation, the population of the energy levels of the H_2 molecule are described by a single-temperature Boltzmann distribution. To verify this statement, the excitation diagrams for several regions of NGC 6881 (Figure 7) have been calculated using a Boltzmann distribution of states where the column densities are related to the $\nu = 1$, $J = 3$ state by

$$\frac{g_3 N(\nu, J)}{g_J N(1, 3)} = \exp\left(-\frac{E(\nu, J) - E(1, 3)}{kT_{ex}}\right), \quad (1)$$

g_J and g_3 being the statistical weights. This equation

can be rearranged in terms of the flux

$$\frac{F(\nu', J') \nu_{1,0S(1)} A_{1,0S(1)} g_3}{F(1, 3) \nu_{\Delta\nu, \Delta J} A_{\nu', J' \rightarrow \nu'', J''} g_J} = \exp\left(-\frac{E(\nu, J) - E(1, 3)}{kT_{ex}}\right), \quad (2)$$

where $A_{\nu', J' \rightarrow \nu'', J''}$ represent the transition probability, and $F(\nu', J')$ is the observed flux at frequency $\nu_{\Delta\nu, \Delta J}$.

The temperature can be inferred from the slope of the line fitted to the data points in Fig. 7. In NGC 6881, the value of the vibrational excitation temperature, $T_{ex}(\nu)$, is similar to this of the rotational excitation temperature, $T_{ex}(J)$, and thus it can be concluded that shocks are the dominant excitation mechanism of H_2 . The excitation temperature is 2100 K for the central region, 2200 ± 100 K for the ionized and H_2 lobes, and 2700 ± 100 K for the extension of the NW H_2 lobe. There is thus, a trend for the temperature to increase as we move farther from the central regions of NGC 6881.

4. DISCUSSION

4.1. Ionized and Molecular Gas in NGC 6881

The H_2 emission of bipolar PNe is typically found in their equatorial rings and on the walls of their bipolar lobes, outlining closely the distribution of ionized material shown in $H\alpha$ or $[\text{N II}]$ images (Kastner et al. 1996; Guerrero et al. 2000). In NGC 6881, however, the different spatial distributions of ionized material and molecular hydrogen trace distinct nebular structures. A search in the literature shows that there are very few cases of bipolar PNe and proto-PNe in which the H_2 and $H\alpha$ or $[\text{N II}]$ morphologies are different: CRL 2688, M 2-9, NGC 2440, NGC 7027, J 900, and Hb 12. From this short list, NGC 2440 has to be discarded as recent *HST* images

(Proposal ID. 11090) have shown that the H_2 arc seen by Latter et al. (1995) follows the outermost $H\alpha$ emission. In CRL 2688 (the Egg Nebula), the H_2 emission is distributed along the equatorial plane and at the tips of the bipolar lobes seen in scattered light (Latter et al. 1993; Sahai et al. 1998). The H_2 bipolar lobes of M 2-9 envelop the bipolar lobes seen in emission lines of ionized species such as Fe II (Smith et al. 2005). The four-lobed shell of H_2 in NGC 7072 surrounds its elliptical ionized core, revealing the location of a photodissociation region (PDR) that is excited by the absorption of UV photons (Hora et al. 1999; Latter et al. 2000). In J 900, the H_2 emission shows a linear structure extending $\sim 40''$ that ends in an arc-like structure (Shupe et al. 1995; Latter et al. 1995). This feature has been suggested to be caused by UV excitation of stellar radiation that leaks out through holes in the nebular envelope (Shupe et al. 1995). Finally, the inner ionized bipolar lobes of Hb 12 are surrounded by an H_2 eye-shaped structure that is interpreted as a broad equatorial ring and a larger pair of bipolar lobes (Hora & Latter 1996; Welch et al. 1999; Kwok & Hsia 2007).

Therefore, among the “exclusive” group of PNe with different distributions of H_2 and ionized gas, M 2-9, Hb 12, and NGC 6881 have ionized bipolar lobes that are enclosed within H_2 bipolar lobes. We note, however, that Hb 12 is a notable case of UV-excited fluorescent H_2 emission (Luhman & Rieke 1996; Hora & Latter 1996) and the same is suspected for M 2-9 (Smith et al. 2005), while NGC 6881 is representative of collisionally excited H_2 emission. The presence of multiple pairs of bipolar lobes in PNe is further discussed in the following section.

4.2. Multiple Bipolar Ejections in NGC 6881

The occurrence of multiple ejections of material is common among PNe, particularly among type I multiple-shell PNe that show faint, giant haloes (Chu et al. 1987). The haloes, interpreted as the relic of late thermal-pulse episodes (Stanghellini & Pasquali 1995; Hajian et al. 1997), are mainly associated with elliptical or round PNe, but are rare among bipolar PNe. Recurrent bipolar ejections resulting in multiple independent pairs of bipolar lobes have been reported for only a handful of PNe. The different pairs of bipolar lobes may have similar morphology and orientation, e.g., M 2-9 (Balick 1999; Schwarz et al. 1997), but in most cases they show notable differences, either affecting their morphology and degree of collimation, e.g., Mz 3 (Guerrero et al. 2004; Santander-García et al. 2004), the orientation of their symmetry axes, e.g., M 2-46 (Manchado et al. 1996), or its ionization degree, e.g., Hb 12 (Welch et al. 1999). In NGC 6881, we find two pairs of highly collimated ionized lobes oriented along slightly different directions and a pair of H_2 bipolar lobes with an open hourglass morphology.

The two pairs of ionized lobes of NGC 6881, first reported by Manchado et al. (1996), have been described in detail by Guerrero & Manchado (1998) and Kwok & Su (2005). Precession is evidenced by the different symmetry axes of each pair of ionized lobes and from the alignment between the equatorial ring and the youngest pair of bipolar lobes. The sharp morphology, similar kinematical age, and different orientation of the

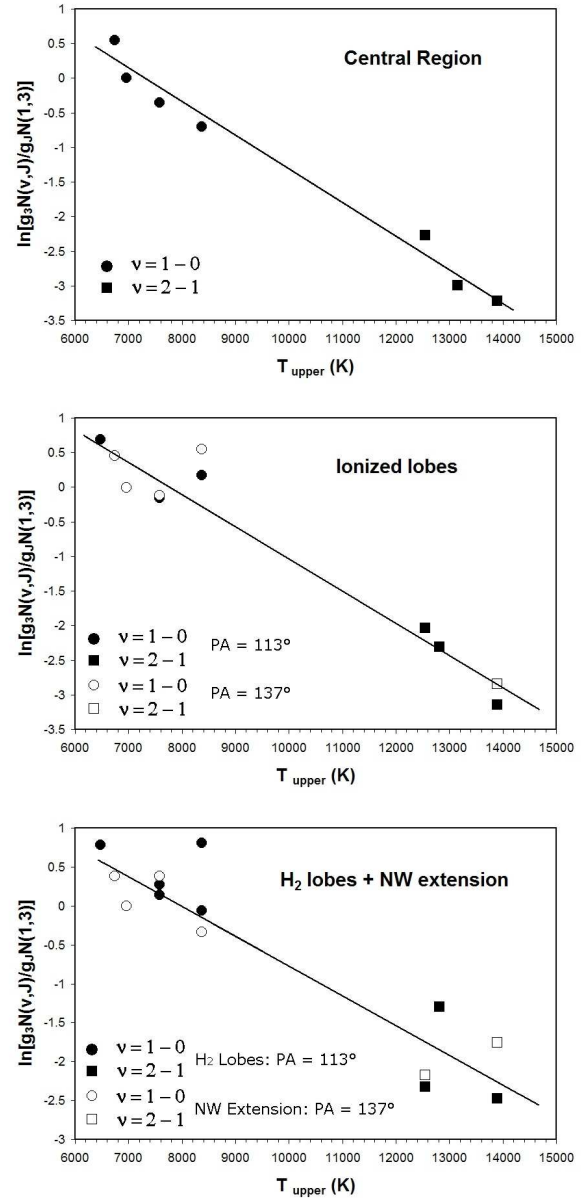


FIG. 7.— Excitation diagrams for the central region (*top*), ionized lobes (*center*), and H_2 -dominated lobes and northwest extension (*bottom*) of NGC 6881. The diagrams show the upper state vibration-rotation populations relative to the $\nu=1$, $J=3$ level plotted against the upper state energy. The linear fits to the populations of different vibrational levels find rotational excitation temperatures of 2000 K, 2100 K, and 2700 K for the central region, ionized lobes, and H_2 -dominated lobes and northwest extension, respectively.

two pairs of bipolar lobes point to a sudden collimated ejection of material that has carved out bipolar cavities into the surrounding medium. The morphology of the ionized bipolar lobes of NGC 6881 is very reminiscent of the proto-PN CRL 618 in which high-velocity jets moving along different directions (Cox et al. 2003) have produced bipolar cavities in the nebular envelope (Trammell & Goodrich 2002). The similarities between the two bipolar nebulae extend to the coaxial rings of the bipolar cavities and to the bright, compact knots at their tips. The collimated outflows of CRL 618 might well evolved in the future into bipolar lobes similar to

those of NGC 6881.

The limb-brightened morphology of the H_2 lobes indicates that the material is mainly confined in their walls, thus suggesting that the bipolar lobes carry enough momentum to sweep up and press the circumstellar medium into a thin sheet. Indeed, the prevalent shock excitation of H_2 requires a source of momentum. It is unlikely that a current fast ($\sim 1000 \text{ km s}^{-1}$) wind from the central star would provide this momentum, as such a stellar wind would be trapped by the inner ionized lobes. Our spectra do not provide information on the expansion velocity of the H_2 lobes, but an upper limit can be derived assuming that the $[N \text{ II}]$ emission from the loop-like structure at the edge of the southeast lobe is produced by a shock. For a planar shock to be able to produce significant $[N \text{ II}] \lambda 6584 \text{ \AA}$ emission, but low or minimal $[O \text{ III}] \lambda 5007 \text{ \AA}$ emission (Guerrero & Manchado 1998), the shock velocity must not exceed $\sim 60 \text{ km s}^{-1}$ (Hartigan, Raymond & Hartmann 1987). Such high speed makes unlikely the origin of the momentum in the thermal pressure of hot gas within the bipolar lobes. However, the momentum of the H_2 bipolar lobes must have been provided at the ejection time, either in a sudden bipolar ejection or through a stellar wind intrinsically bipolar or isotropic but collimated by an equatorial structure. The oblique shock of a bipolar lobe expanding at $\sim 60 \text{ km s}^{-1}$ would be able to shock excite the H_2 molecules along its edge, while giving rise to $[N \text{ II}]$ and $H\alpha$ emission at its tip. Such ballistic ejection may also explain the increasing H_2 temperature excitation with the distance to the nebula center.

The very different collimation degree of the ionized and H_2 lobes of NGC 6881 suggests that they formed during two different ejection events with substantial changes in the collimation conditions or even in the collimation mechanisms between the two episodes. The H_2 lobes formed very likely by the action of an episodic wind producing an hourglass-shaped ejection, while high velocity jets ejected along close directions produced the two pairs of ionized lobes. An additional period of isotropic heavy mass loss resulting in a dense envelope is revealed by concentric arcs detected around the innermost regions of NGC 6881 (Corradi et al. 2004).

4.3. NGC 6881 and the Surrounding Interstellar Medium

The morphology of the southeast and northwest H_2 -dominated bipolar lobes are discrepant, with the former being smaller than the latter and showing a sharp edge at its southeast tip. This sharp edge is spatially coincident with a $[N \text{ II}]$ loop-like feature (Fig. 4), a structure that has been interpreted as a low velocity precessing jet (Guerrero & Manchado 1998), but that, in view of the perfect spatial coincidence with the southeast tip of the H_2 lobe, seems more likely to mark its termination. The abrupt border of the southeast H_2 lobe and the $[N \text{ II}]$ loop-like structure may unveil the interaction of this bipolar lobe with dense material.

As we noted in §3.1, NGC 6881 is embedded within diffuse emission that forms part of Sh 2-109, an inhomogeneous $H \text{ II}$ region located at a distance of $1.4 \pm 0.4 \text{ kpc}$ and with a diameter of $400 \pm 100 \text{ pc}$ (Fich & Blitz 1984). In view of the hint of interaction of the southeast H_2 lobe of NGC 6881 with dense material, result-

ing in the notably different morphologies of the southeast and northwest lobes, it is worthwhile to investigate the physical association of NGC 6881 with Sh 2-109. The distance to NGC 6881 has been estimated to be 2.5 kpc by Cahn, Kaler & Stanghellini (1992) who used the Shklovsky method according to the Daub scheme. In their work, Cahn et al. used an angular radius of $2''.5$ which seems inadequate as it only traces the bright, central regions of NGC 6881. This region has an angular radius $\sim 1''.2$, but if we account for the ionized bipolar lobes, then an averaged angular radius of $6''.5$ has to be used. If we adopt this radius, then the revised distance to NGC 6881 using the Cahn et al. method would be $\sim 1.5 \text{ kpc}$, supporting its physical association with the $H \text{ II}$ region Sh 2-109.

An inspection of IPHAS $H\alpha$ images of this region reveals that the diffuse emission in which NGC 6881 is embedded constitutes the eastern wall of a large cavity-like structure. $H \text{ I}$ 21 cm line observations of the neutral gas distribution and kinematics of the region confirm that this structure is a cavity with an expansion velocity $\sim 10 \text{ km s}^{-1}$ (Cappa et al. 1996). The radial velocity of this $H \text{ I}$ cavity, $v_{\text{LSR}} \sim +16 \text{ km s}^{-1}$, is very similar to the radial velocity of NGC 6881, $v_{\text{LSR}} \sim +2 \text{ km s}^{-1}$ (Guerrero & Manchado 1998). The projection of the nebula onto the $H \text{ I}$ cavity and their similar radial velocities suggest that NGC 6881 may be located within this cavity, with its H_2 -dominated southeast lobe hitting onto the dense material at the wall of the cavity, slowing it down and producing a sharp edge, while the northwest H_2 lobe expands into the $H \text{ I}$ cavity with little opposition.

5. CONCLUSIONS AND SUMMARY

New images and near-IR spectra of NGC 6881 confirm the different distribution of ionized material and molecular hydrogen within this PN. The H_2 images have resolved its central region which shows the spatial distribution expected for a ring of molecular material surrounding an innermost ionized ring. The H_2 bipolar lobes share the same orientation than the ionized lobes, but they are less collimated and display a distinct hourglass morphology. The H_2 emission is predominantly shock excited, both in the central ring and in the H_2 bipolar lobes.

We infer a complex history formation for NGC 6881, involving important changes in the collimation mechanism of the bipolar lobes in the latest evolutionary stages. The H_2 bipolar lobes are consistent with the action of a bipolar wind. The final evolution of the PN implied the ejection of episodic fast collimated outflows with changing directions that interacted with the dense circumstellar envelope ejected in a previous phase.

The southeast H_2 lobe of NGC 6881 is less extended than the northwest lobe and shows a sharp edge, implying the interaction of NGC 6881 with an inhomogeneous interstellar medium. We find very likely that NGC 6881 is within a cavity in the midst of the $H \text{ II}$ region Sh 2-109.

This work is funded by grant PNAYA2005-01495 of the Spanish MEC. G.R.L. thanks the IAA for its hospitality and the support of a postgraduate scholarship from CONACyT (Mexico). We thank J. Acosta and G. Gómez for taking the LIRIS images of NGC 6881, and K. Viironen and the IPHAS team for providing us with large-scale $H\alpha$ images of the region around NGC 6881.

We are also grateful to E.J. Alfaro for enlightening dis-

cussion on the location of NGC 6881 within the Galaxy.

REFERENCES

- Balick, B. 1987, *AJ*, 94, 617
 Balick, B. 1999 ASP Conference Series, 188 *Optical and Infrared Spectroscopy of Circumstellar Matter*, eds. E., Guenther, B., Stecklum, & S., Klose, (San Francisco, CA:ASP), 241
 Black, J.H., & van Dishoeck, E.F. 1987, *ApJ*, 322, 412
 Bond, H.E. 2000, in *Asymmetrical Planetary Nebulae II: From Origins to Microstructures*, ed. J.H. Kastner, N. Soker & S. Rappaport, ASP Conf. Ser. 199, (San Francisco, CA:ASP), 115
 Burton, M.G., Brand, P.W.J.L., Geballe, T.R., & Webster, A.S. 1989, *MNRAS*, 236, 409
 Cahn, J.H., Kaler, J.B., & Stanghellini, L. 1992, *A&AS*, 94, 399
 Cappa, C. E., Dubner, G. M., Rogers, C., & St-Louis, N. 1996, *AJ*, 112, 1104
 Chu, Y.-H., Jacoby, G.H., & Arendt, R. 1987, *ApJ*, 64, 529
 Corradi, R.L.M., & Schwarz, H.E 2005, *A&A*, 293, 871
 Corradi, R.L.M., Guerrero, M., Manchado, A. & Mampaso, A. 1997, in *IAU Symp. 180 Planetary Nebulae*, eds. H.J. Habing & H.J.G.L.M. Lamers (Dordchet: Kluwer Academic), 216
 Corradi, R.L.M., Sanchez-Blázquez, P., Mellema, G., Gianmanco, C., & Schwarz, H.E 2004, *A&A*, 417, 637
 Cox, P., Huggins, P.J., Maillard, J.-P., Muthu, C., Bachiller, R. & Forveille, T. 2003, *ApJ*, 568, L87
 Drew, J. E., et al. 2005, *MNRAS*, 362, 753
 Fich, M., & Blitz, L. 1984, *ApJ*, 508, 262
 Guerrero, M. A., Chu, Y.-H., & Miranda, L.F. 2004, *AJ*, 128, 1694
 Guerrero, M. A., & Manchado, A. 1998, *ApJ*, 279, 125
 Guerrero, M. A., Manchado, A., & Serra-Ricart, M. 1996, *ApJ*, 456, 651
 Guerrero, M. A., Villaver, E., Manchado, A., García-Lario, P., & Prada, F. 2000, *ApJS*, 127, 125
 Hajian, A.R., Frank, A., Balick, B., & Terzian, Y. 1996, *ApJ*, 477, 226
 Hartigan, P., Raymond, J., & Hartmann, L. 1987, *ApJ*, 316, 323
 Hora, J.L., & Latter, W.B., 1996, *ApJ*, 461, 288
 Hora, J.L., Latter, W.B., & Deutsch, L.K. 1999, *ApJS*, 124, 195
 Hunt, L. K., Mannucci, F., Testi, L., Migliorini, S., Stanga, R. M., Baffa, C., Lisi, F., & Vanzì, L. 1998, *AJ*, 115, 2594
 Kastner, J.H., Weintraub, D.A., Gatley, I., Merrill, K.M., & Probst, R.G. 1996, *ApJ*, 462, 777
 Kwok, S., Purton, C.R., & Fitzgerald, P.M. 1978, *ApJ*, 219, L125
 Kwok, S., & Su, K.Y.L. 2005, *ApJ*, 635, L49
 Kwok, S., & Hsia, C.H. 2007, *ApJ*, 660, 341
 Latter, W.B., Dayal, A., Bieging, J.H., Meakin, C., Hora, J.L., Kelly, D.M., & Tielens, A.G.G.M. 2000, *ApJ*, 539, 783
 Latter, W. B., Hora, J. L., Kelly, D. M., Deutsch, L. K., & Maloney, P. R. 1993, *AJ*, 106, 260
 Latter, W.B., Kelly, D.M., Hora, J.L., & Deutsch, L.K. 1995, *ApJS*, 100, 159
 López, J.A., Meaburn, J., Bryce, M., & Holloway, A.J. 1998 *ApJ*, 493, 803
 Luhman, K. L., & Rieke, G. H. 1996, *ApJ*, 461, 298L
 Manchado, A., Guerrero, M. A., Stanghellini, L., & Serra-Ricart, M. 1996, *The IAC Morphological Catalog of Northern Galactic Planetary Nebulae*, (Tenerife:IAC)
 Manchado, A., Stanghellini, L., & Guerrero, M.A. 1996, *ApJ*, 466, L95
 Miranda, L.F., Guerrero M. A., & Torrelles, J.M. 1999, *ApJ*, 117, 1421
 Parker, R.A.R., Gull, T.R., & Kirshner, R.P. 1979, *An Emission Line Survey of the Milky Way* (NASA SP-434)
 Sahai, R. 1998, *ApJ*, 537, L43
 Sahai, R., Hines, D. C., Kastner, J. H., Weintraub, D. A., Trauger, J. T., Rieke, M. J., Thompson, R. I., & Schneider, G. 1998, *ApJ*, 492, L163
 Sahai, R., & Trauger, J.T. 1998, *AJ*, 116, 1357
 Santander-García, M., Corradi, R.L.M., Balick, B., & Mampaso, A. 2004, *A&A*, 426, 185
 Schwarz, H.E., Aspin, C., Corradi, R.L.M., & Reipurth, B. 1997, *A&A*, 319, 267
 Shupe, D.L., Armus, L., Matthews, K., & Soifer, B.T. 1995, *AJ*, 109, 1173
 Smith, N., Balick, B., & Gehrz, R. D. 2005, *AJ*, 130, 853
 Soker, N. 1997, *ApJS*, 112, 487
 Soker, N. 2006, *PASP*, 118, 260
 Sørensen, P., & Pollacco, D. 2004 in *Asymmetrical Planetary Nebulae III: Winds, Structure and the Thunderbird*, ed. M. Meixner, J.H. Kastner, B. Balick & N. Soker, ASP Conf. Ser. 313 (San Francisco, CA:ASP), 515
 Stanghellini, L., & Pasquali, A. 1995, *ApJ*, 452, 286
 Trammell, S.R., & Goodrich, R.W. 2002, *ApJ*, 579, 688
 Welch, C.A., Frank, A., Pipher, J.L., Forrest, W.J., & Woodward, C.E. 1999, *AJ*, 522, L69